Further investigation on the fusion of ^{6}Li with ^{209}Bi target at near-barrier energies*

G. L. Zhang (张高龙)[1] Z. W. Jiao (焦振威)[1] G. X. Zhang (张广鑫)[2†] M. R. Cortes[3] S. P. Hu (胡世鹏)[4,5‡]
J. Q. Qian (钱建强)[1] D. Mengoni[6,7] W. W. Qu (屈卫卫)[8] C. B. Li (李聪博)[9] Y. Zheng (郑云)[9]
H. Q. Zhang (张焕乔)[9] H. B. Sun (孙慧斌)[4,5] N. Wang (王楠)[4] C. L. Zhang (张春雷)[10] J. J. Valiente-Dobón[11]
D. Testov[7] M. Mazzocco[6,7] A. Gozzelino[11] C. Parascandolo[12] D. Pierroutsakou[12] M. La Commara[12,13]
A. Goasduff[11] D. Bazzacco[6] D. R. Napoli[11] F. Galtarossa[6] F. Recchia[6,7] A. Illana[11] S. Bakes[11] I. Zanon[11]
S. Aydin[14] G. de Angelis[11] M. Siciliano[11,15] R. Menegazzo[6] S.M. Lenzi[6,7] J. L. Ferreira[3] J. Rangel[16,3]
Serkan Akkoyun[17] L. F. Canto[18] J. Lubian[3§]

[1]School of Physics, Beihang University, 100191 Beijing, China
[2]Sino-French Institute of Nuclear Engineering and Technology, Sun Yat-Sen University, Zhuhai 519082, Guangdong, China
[3]Instituto de Física, Universidade Federal Fluminense, 24210-340, Niterói, Rio de Janeiro, Brazil
[4]Institute for Advanced Study in Nuclear Energy & Safety, Shenzhen University, China
[5]Shenzhen Key Laboratory of Research and Manufacture of High Purity Germanium Materials and Fetectors, Shenzhen University, 518060
[6]INFN, Sezione di Padova, Padova, Italy
[7]Dipartimento di fisica Astronomia dell'Universita di padova, Padova, Italy
[8]State Key Laboratory of Radiation Medicine and Protection, School of Radiation Medicine and Protection, Soochow University, Suzhou 215123, China
[9]China Institute of Atomic Energy, Beijing 102413, China
[10]The Key Laboratory of Beam Technology and Material Modification of Ministry of Education, College of Nuclear Science and Technology, Beijing Normal University, Beijing 100875, China
[11]INFN, Laboratori Nazionali di Legnaro, I-35020 Legnaro, Italy
[12]INFN, Sezione di Napoli, I-80126 Napoli, Italy
[13]Dipartimento di Farmacia, Universita di Napoli "Federico II", I-80131 Napoli, Italy
[14]Department of Natural and Mathematical Sciences, Faculty of Engineering, Tarsus University, 33480 Mersin, Turkiye
[15]Physics Division, Argonne National Laboratory, Lemont-IL, USA
[16]Departamento de Matemaética, Física e Computaç˜ao Universidade do Estado do Rio de Janeiro, Faculdade de Tecnologia, 27537-000, Resende, Rio de Janeiro, Brazil
[17]Department of Physics, Sivas Cumhuriyet University, Sivas, Turkey
[18]Instituto de Física, Universidade Federal do Rio de Janeiro, CP 68528, 21941-972, Rio de Janeiro, Brazil

CPC Accepted

Abstract: The complete and incomplete fusion cross sections for ^{6}Li+^{209}Bi were measured via the in-beam γ-ray method around the Coulomb barrier. The cross sections of (deuteron captured) incomplete fusion (ICF) products were re-quantified experimentally for this reaction system. The results reveal that the ICF cross section is equivalent to that of complete fusion (CF) above the Coulomb barrier and dominant near or below the Coulomb barrier. A theoretical calculation based on the Continuum Discretized Coupled Channel (CDCC) method is performed for the aforementioned CF and ICF cross sections, and the result is consistent with the experimental ones. The universal fusion function (UFF) is also compared with the measured CF cross section with different barrier parameters, demonstrating that the CF suppression factor is quite sensitive to the choice of potential, which can reflect both dynamic and static effects of breakup on the fusion process.

Keywords: cross section, incomplete fusion, suppression factor, weakly bound nuclei

DOI:

Received 14 March 2024; Accepted 23 April 2024

* This work is supported by the National Nature Science Foundation of China under Grants No. 11975040, No. U2167204, and No. 1832130. This work is partially supported by (M.S.) the U.S. Department of Energy, Office of Science, Office of Nuclear Physics, under contract number DE-AC02-06CH11357. This work is also supported By Guangdong Key Research And Development Program 2020B040420005; LingChuang Research Project of China National Nuclear Corporation 20221024000072F6-0002-7 Nuclear Energy Development and Research Project 202203-SZU. The work is also supported by the '111' center (B20065)

† E-mail: zhanggx37@mail.sysu.edu.cn
‡ E-mail: husp@szu.edu.cn
§ E-mail: jlubian@id.uff.br

©2024 Chinese Physical Society and the Institute of High Energy Physics of the Chinese Academy of Sciences and the Institute of Modern Physics of the Chinese Academy of Sciences and IOP Publishing Ltd

I. INTRODUCTION

The stable weakly-bound nuclei, such as ^{6}Li, ^{7}Li, and ^{9}Be, have low binding energies and strong cluster structures. They frequently undergo a breakup reaction before fusing with the target nucleus, leading to various reaction channels. If the target captures the whole projectile without breakup, it is called direct complete fusion (DCF). If the projectile breakup and all fragments are captured successively by the target, it is regarded as sequential complete fusion (SCF). The complete fusion cross section is the sum of DCF and SCF. The incomplete fusion means that only parts of fragments are captured by the target. It should be noted here that the cluster-transfer reaction would lead to the same residuals with ICF, being indistinguishable from the cross section measurement.

The detailed reaction mechanism induced by weakly bound nuclei has been a hot topic during recent decades [1, 2], especially when one notices that a lot of experiments have been performed, such as ^{6}Li, ^{7}Li, and ^{9}Be on the ^{24}Mg [3], ^{28}Si [4], ^{96}Zr [5],^{197}Au [6], ^{198}Pt [7], ^{209}Bi [8, 9] and ^{208}Pb [9] targets. From the experimental point of view, the measurement of ICF cross sections would be difficult since the ICF residues have a significant overlap with the one from the CF channel (via the evaporation of charged particles). Therefore, one has to go for a heavy target nucleus system in which the evaporation of charged-particle is usually very small (also predicted by statistical models such as PACE [10−12]). For instance, Dasgupta et al. [13, 14] have measured the CF and ICF cross sections for the ^{6}Li+^{209}Bi reaction by detecting the α decay events from different residues. Unfortunately, they were unable to obtain an accurate deuteron-captured ICF (d-ICF) reaction cross section. On one hand, certain important products cannot be measured in this manner due to their long lifetime in ground state, such as ^{209}Po with a half-life of 102 years. Besides, some products, such as ^{210}Po, have a decay chain crossover, resulting in an excessively large cross section. In the present work, CF and ICF cross sections for the ^{6}Li+^{209}Bi system are re-measured by in-beam γ-ray measurement. Compared to α decay measurements, this approach provides a more complete deuteron-captured ICF (d–ICF) reaction cross section, which can give a comprehensive picture of the reaction mechanism induced by weakly bound projectile. Furthermore, charged particle measurements can be performed simultaneously with in beam γ-ray measurements, allowing for charged particle-γ coincidence measurements and the identification of various reaction channels.

From the theoretical point of view, a CDCC-based method has been recently used to reproduce the CF and ICF cross sections induced by ^{6,7}Li [15, 16] on heavy targets. The fusion process in this method is viewed as the collision between the projectile (P), which consists of two clusters (c1 and c2), and the spherical target (T). To handle the interactions between the target and each cluster in the projectile independently, the CDCC approach is required. This method works quite well in the description of CF cross sections of the ^{6}Li + ^{124}Sn, ^{197}Au, ^{198}Pt, and ^{209}Bi systems. Nevertheless, it lacks experimental data support, especially for ICF data, including the ^{6}Li+^{209}Bi system.

This paper is organized as follows: Sec. II introduces the experimental setup. Sec. III shows the data analysis and experimental results. Sec. IV and Sec. V demonstrates the theoretical methods and comparisons between the results of the theoretical calculations and the experimental data, respectively. The summary is given in Sec. VI.

II. EXPERIMENTAL SETUP

The ^{6}Li+^{209}Bi experiment was performed at Legnaro National Laboratories, Italy. A 550-μg/cm^2 ^{209}Bi target backed with a 110-μg/cm^2 ^{12}C foil was bombarded by the ^{6}Li^{3+} beam with an average intensity of 2.0 enA. The beam energies were 28, 30 and 34 MeV in the laboratory frame, corresponding to around 0.99, 1.06, and 1.21 times the Coulomb barrier (derived using the São Paulo potential(SPP) [17, 18]), respectively.

The GALILEO (Gamma Array of Legnaro INFN Laboratories for nuclEar spectrOscopy) array [19] was used to measure the γ transition from different fusion-evaporation residues. The array is composed of 25 Compton-suppressed HPGe tapered detectors, which are organized in 4 rings at 152°, 129°, 119°, and 90° concerning the beam direction. There are five detectors in each ring at backward angles, and the last ring at 90° has ten detectors. The distance from the target to the detector is 22.7 cm. The total measured full-energy-peak efficiency was 1.83% at 1408 keV. The energy resolution was 0.20% at 1408 keV transition of ^{152}Eu calibration source (FWHM = 2.88 keV). Inside the GALILEO, the EUCLIDES (EUroball Charged Light particle Identification DEtector Sphere) [20], a ΔE-E telescope array of 40 silicon detectors, was employed for light-charged particle identification. The ΔE and E layers are 130 and 1000 μm thick, respectively. The distance between the ΔE detector and the target is 62 mm. A typical two-dimensional spectrum obtained at the angular ranges covered by the absorber at E_{beam} = 34 MeV is shown in Fig. 1, in which protons, deuterons, tritons, and alphas labeled as p, d, t, and α can be clearly identified. To protect the detector from the intense scattering beam, an aluminum cylindrical absorber was inserted inside the EUCLIDES along the beam direction. The particle-γ coincidence method was used in this work to identify the different reaction channels. When the beam energy was 34 MeV, the thickness of the cylinder was set to 146 μm, and the backward

CPC Accepted

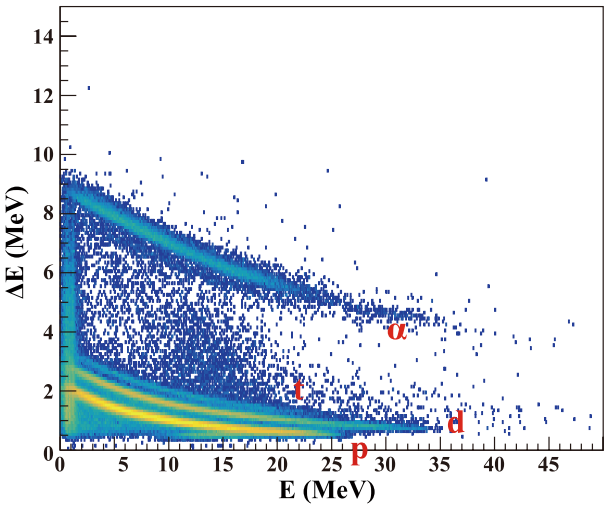

Fig. 1. (color online) The two-dimensional correlation plot of ΔE vs E for identification of light charged particles at 30 MeV. p, d, t, α denote proton, deuteron, triton, and alpha particles, respectively.

angles larger than 90° were unshielded by the absorber. In the case of 30 MeV and 28 MeV, the aluminum absorber covered all angles but with a thickness of 138 μm at the 90° and forward angles and 110 μm at the backward angles. The beam intensity was recorded by a Faraday cup (FC) placed 3 m behind the target. The schematic of the experimental setup is shown in Fig. 2. A detailed description of the experimental setup can be found in Refs. [19, 20].

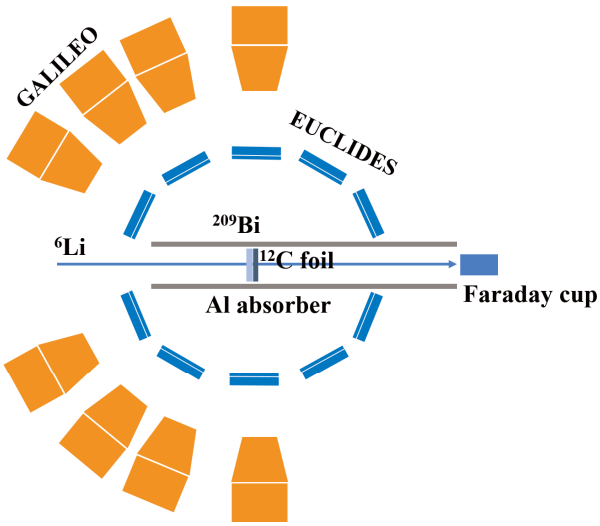

Fig. 2. (color online) The schematic of the experimental setup (sectional view). HPGe detectors and ΔE-E telescopes present the schematic of a part of GALILEO and EUCLIDES arrays, respectively. For details, see the text.

III. EXPERIMENTAL RESULTS

In the ^{6}Li+^{209}Bi reaction, the compound nucleus of the complete fusion process is ^{215}Rn, producing lighter Rn isotopes by evaporating different numbers of neutrons. Similarly, the products of α-ICF and d−ICF are At and Po isotopes, respectively. The typical in-beam γ-ray spectrum for the ^{6}Li+^{209}Bi reaction system at E_{beam} = 34 MeV is shown in Fig. 3 (a), where the identified γ lines of different Rn, At, and Po isotopes are denoted. The rays used to determine the cross section are marked in blue, and the rays of other fusion and transfer products are marked in black. The reaction products of ^{6}Li with ^{12}C and ^{27}Al are marked in red. The major products of the CF reaction are ^{212}Rn and ^{211}Rn. For d−ICF, the main products are ^{210}Po and ^{209}Po. For α-ICF, the main residues include ^{212}At and ^{211}At. Figs. 3 (b)-(g) show the single γ-ray spectra ((b)-(d), zoom-in parts of (a)) and the ones gated on deuteron ((e)-(g)) within specific energy regions, respectively. It can be seen that when gated on the measured deuteron, the γ-ray spectra show characteristic γ lines in At isotopes, being related to α-capture ICF process. From the comparison, it can be concluded that even though weak, the lower limits of cross section for At isotopes can be obtained since several characteristic γ lines can be observed in the singles γ-ray spectra and more significant in the deuteron gated ones.

In the present work, all the observed γ transitions feeding (directly) the ground state or long-lived isomers are collected to determine the yield of the specific isotope. Detailed information about the γ transitions and related information in each nucleus is summarised in Table 1 [21−26]. In such a situation, only the production of excited states in the evaporation residues can be measured, and the cross sections can be determined as follows:

$$\sigma = \frac{1}{N_B N_T}\left[\sum_{i=1}^{n}\frac{A_{E_{\gamma i}}\left(1+F_{E_{\gamma i}}\right)}{\varepsilon_{E_{\gamma i}}}\right]. \quad (1)$$

Here n represents the number of the γ transitions directly feeding the ground state or long-lived isomer in the same residue. $A_{E_{\gamma i}}$ is the counts of measured γ rays with energy $E_{\gamma i}$. $\varepsilon_{E_{\gamma i}}$ accounts for the efficiency. $F_{E_{\gamma i}}$ is the inner conversion electron rate. N_B and N_T are the numbers of beam particles and target nuclei, respectively. The total uncertainty for the cross sections measurement comes from (1) statistical errors associated with the yields of γ-rays, (2) errors in the determination of absolute efficiency, (3) the error in the beam intensity normalization process, includes the experimental error of ^{212}Rn in Ref. [14]., and (4) uncertainty in the target thickness. The overall error bar ranges from 7% at E_{beam}=34 MeV to nearly 14% at E_{beam}=28 MeV.

However, due to the existence of dark currents from the Faraday cup, the beam intensity measurement be-

CPC Accepted

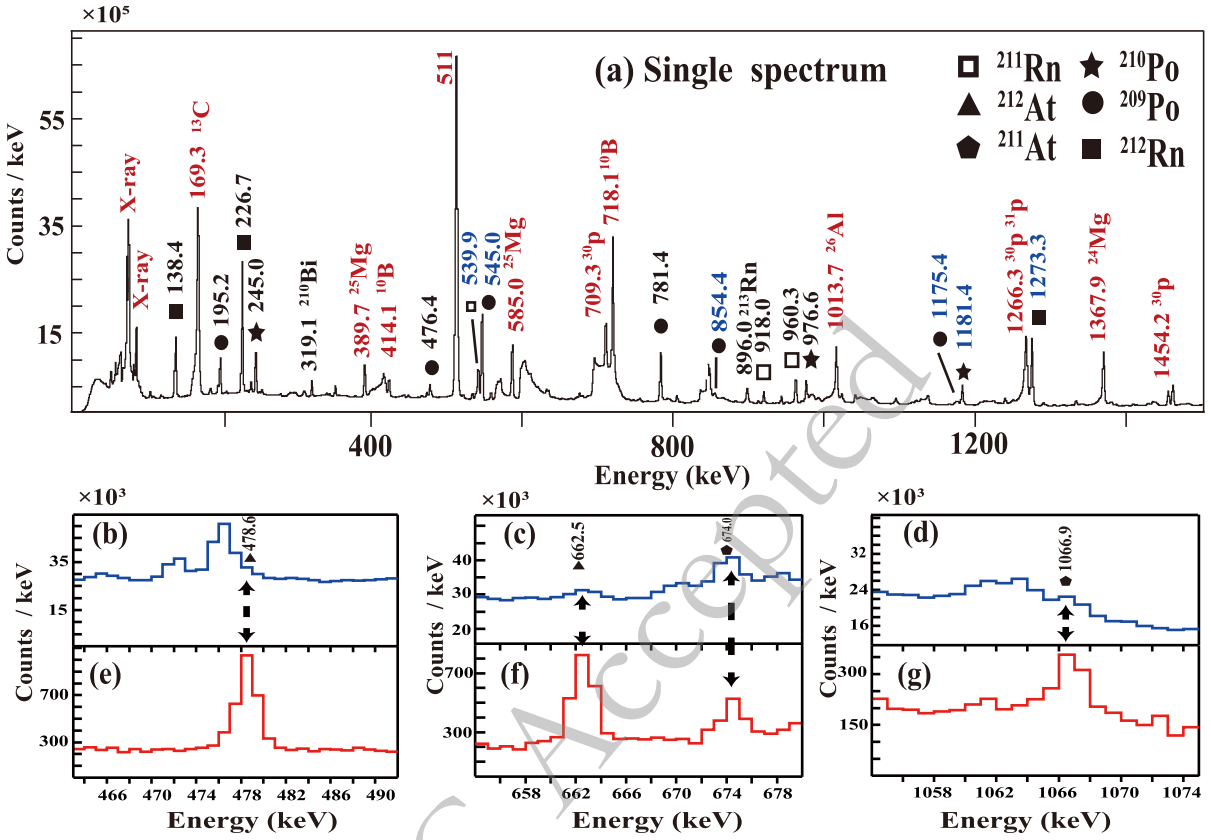

Fig. 3. (color online) (a) In-beam γ-ray spectrum for ^{6}Li+^{209}Bi system at 34 MeV. The rays used to determine the cross section are marked in blue, and the rays of other fusion and transfer products are marked in black. The reaction products of ^{6}Li with ^{12}C and ^{27}Al are marked in red. (b)-(g) compare the single γ-ray spectra ((b)-(d)) with the ones gated on deuteron ((e)-(g)) within specific energy regions, stressing the fact that even though weak, several characteristic γ lines in At isotopes can still be measured in the present experiment.

Table 1. Reaction channels and characteristic γ rays counted in the ^{6}Li+^{209}Bi system.

Residual channels	Transition	E_γ (keV)
^{211}Rn(CF, 4n)	$5/2^- \rightarrow 1/2^-$	539.9
^{212}Rn(CF, 3n)	$2^+ \rightarrow 0^+$	1273.7
^{209}Po(d−ICF, 2n)	$5/2^- \rightarrow 1/2^-$	545.0
	$3/2^- \rightarrow 1/2^-$	854.4
	$5/2^- \rightarrow 1/2^-$	1175.4
^{210}Po(d−ICF, 1n)	$2^+ \rightarrow 0^+$	1181.4
^{211}At(α-ICF, 2n)	$13/2^- \rightarrow 9/2^-$	1066.9
	$7/2^- \rightarrow 9/2^-$	674.0
^{212}At(α-ICF, 1n)	$11^+ \rightarrow 9^-$	662.5
	$10^- \rightarrow 9^-$	478.6

comes unreliable in the present experiment. As mentioned in the introduction part, the same ^{6}Li+^{209}Bi experiment has been done before with a different method [14] in which the beam intensities were measured precisely. In the present paper, one specific isotope, ^{212}Rn (the one with the highest cross sections among CF residues for all the energies used in this experiment, see Table 2 in Ref. [14]), is employed for the normalization of beam intensity. As a result, the identical cross sections for ^{212}Rn concerning Ref. [14] are obtained in this work (shown in Table 2) for the same energies, here it should be mentioned that the error bar is independent for each work. With the normalized beam intensity, all the measured cross sections for each isotope in this experiment are displayed in Table 2 and Fig. 4. It should be mentioned again that such an in-beam γ-ray method can only collect the transitions feeding the ground states or long-live isomer, giving rise to a lower limit for the cross section since the part that directly populates the ground state or long-lived excited states cannot be considered.

The CF cross sections are fairly consistent with previous results in Ref. [14], confirming the feasibility of the present measurement. However, the α−ICF cross section is the lower bound for this quantity. This is due to the underestimation of the cross section of ^{212}At. The complete measurement of the ^{212}At cross section is now impossible because many transitions feeding ground state or long-

CPC Accepted

Table 2. Experimental integrated cross sections of each isotope with incident beam energies of 28, 30, 34 MeV. The $E_{c.m.}$ is corrected for energy losses in the target.

E_{beam} (MeV)	28	30	34
$E_{c.m.}$ (MeV)	27.11	29.06	32.95
$\sigma_{^{211}Rn}$ (mb)	–	–	39.64 ± 2.89
$\sigma_{^{212}Rn}$ (mb)	4.70 ± 0.68	36.10 ± 2.70	175.20 ± 12.25
σ_{CF} (mb)	4.70 ± 0.68	36.10 ± 2.70	214.84 ± 12.59
$\sigma_{^{209}Po}$ (mb)	19.20 ± 2.67	69.54 ± 4.85	167.49 ± 10.91
$\sigma_{^{210}Po}$ (mb)	17.53 ± 2.53	42.14 ± 3.15	52.84 ± 3.69
σ_{d-ICF} (mb)	36.73 ± 3.67	111.68 ± 5.79	220.33 ± 11.51
$\sigma_{^{211}At}$ (mb)	–	0.71 ± 0.06	13.73 ± 0.91
$\sigma_{^{212}At}$ (mb)	–	2.29 ± 0.15	11.47± 0.77
$\sigma_{\alpha-ICF}$ (mb)	–	3.00 ± 0.16	25.20 ± 1.19

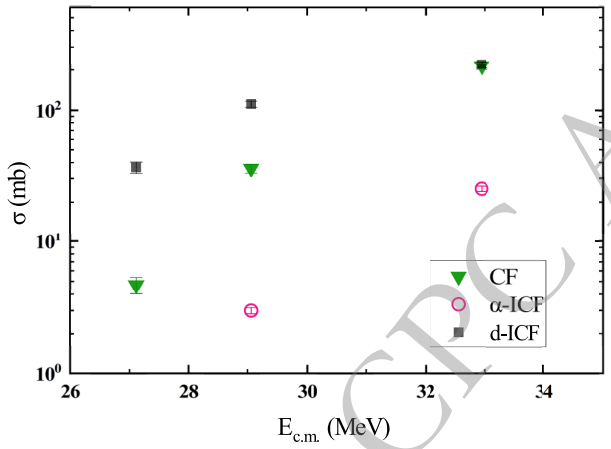

Fig. 4. (color online) The experimental excitation functions of CF and ICF channels.

lived isomers have insufficient intensity during the current experiment. On the other hand, due to the fact that ^{212}At is an odd-odd nucleus, the level scheme is rather complicated, thus there could be any unknown transitions which can feed the ground or long-lived isomeric states in ^{212}At, which are not taken into account in the cross section measurement.

For the $d-$ICF channel, the cross section for ^{209}Po has been measured for the first time with a relatively large value, as shown in Table 2. Conversely, the present work also provides a cleaner cross section for ^{210}Po populated in the fusion process. The reason is explained below. In the ^{6}Li + ^{209}Bi system, the single neutron transfer reaction has an appreciable cross section, producing ^{210}Bi whose ground state undergoes β decay to ^{210}Po. Because ^{210}Bi $\rightarrow$ ^{210}Po β decay channel has a Q value of 1.16 MeV, smaller than the first excited state in ^{210}Po (2^{+} at 1.18 MeV), only one β decay branch can exist, which feeds the ground state in the daughter nucleus. As a result, the measurement of α decay events (de-exciting the ground state of ^{210}Po) would be affected by the production of ^{210}Bi. In the in-beam γ-ray measurement, only γ rays de-exciting the excited states would be collected. Therefore, the existence of ^{210}Bi would not have any influence at all.

Comparing the observed CF and ICF cross sections shown in Fig. 4, it is evident that for the ^{6}Li+^{209}Bi system, CF and ICF are comparable at energies above the Coulomb barrier, but the CF cross section drops more rapidly as energy decreases. The detailed discussion will be performed in Sec. V.

IV. THEORETICAL METHOD

We adopt the theoretical model of Ref. [16] to analyze the CF and ICF data. In this model, the projectile is treated as a system of two clusters, c_1 and c_2, which in the case of ^{6}Li, are respectively ^{2}H and ^{4}He. These clusters are bound by the energy $B = 1.47$ MeV, and the spectroscopic amplitude for this cluster configuration in the g.s. of ^{6}Li was empirically determined in Ref. [16]. The derived value was 0.7 (see Eqs. (16) and (18) of Ref [16]). It is slightly less than 1.0.

The collision dynamics are determined by the full Hamiltonian of the system, given by

$$\mathbb{H}(\mathbf{R},\mathbf{r}) = h(\mathbf{r}) + \hat{T}_{\mathbf{R}} + \mathbb{V}(\mathbf{R},\mathbf{r}) - i\,\mathbb{W}(\mathbf{R},\mathbf{r}), \tag{2}$$

where $h(\mathbf{r})$ is the intrinsic Hamiltonian describing the relative motion of the clusters within the projectile, $\hat{T}_{\mathbf{R}}$ is the kinetic energy operator associated with the center of mass projectile-target relative motion, and $\mathbb{V}(\mathbf{R},\mathbf{r})$ is the real part of the projectile-target interaction, represented by

$$\mathbb{V}(\mathbf{R},\mathbf{r}) = \mathbb{V}^{(1)}(\mathbf{r}_1) + \mathbb{V}^{(2)}(\mathbf{r}_2), \tag{3}$$

where $\mathbb{V}^{(i)}$ stands for the interaction between fragment c_i and target.

In Eq. (2), $\mathbb{W}(\mathbf{R},\mathbf{r})$ is the imaginary potential that should account for the absorption of different fusion processes. To simulate the effects of fusion, one should remember that the imaginary potential should be very absorptive and has a short range. This is equivalent to the so called ingoing-wave boundary condition in BPM calculations, and does not depend on the Woods-Saxon potential [27]. It must ensure total absorption in the inner region of the barrier and should vanish elsewhere.

In the coupled channel method, one carries out a channel expansion of the total wave function of the system, and this expansion should include all channels that are relevant to the collision dynamics. In the case of tightly bound systems, they are labeled by a set of dis-

CPC Accepted

crete quantum numbers, denoted by α. The situation is more complicated in collisions of weakly bound nuclei, where the collision dynamics is strongly influenced by breakup channels. In this case, the channel expansion must also include intrinsic states in the continuum. In this way, α includes a continuous quantum number, ε, corresponding to the relative energy of the clusters. Then, the coupled channel method would lead to infinite coupled equations. To address this issue, one uses the continuum discretized coupled channel (CDCC) approach [28, 29], which consists of replacing the infinite set of states in the continuum by a finite set of wave packets (*bins*), $\phi_n\,(n=1,...,N)$, generated by superposing scattering states between fragments with a definite angular momentum in an energy interval, each one centered at one of the energies of the set $\{\varepsilon_1,....,\ \varepsilon_N\}$. Then, the total wave function of the system, $\Psi^{(+)}(\mathbf{R},\mathbf{r})$, can be expanded in this new basis of states and written as

$$\Psi^{(+)}(\mathbf{R},\mathbf{r}) = \Psi_0(\mathbf{R},\mathbf{r}) + \Psi_{\rm bu}(\mathbf{R},\mathbf{r}), \tag{4}$$

where $\Psi_0(\mathbf{R},\mathbf{r})$ and $\Psi_{\rm bu}(\mathbf{R},\mathbf{r})$, are, respectively, the wave functions of the elastic channel and the breakup wave function within the CDCC approach. Above, $\mathbf{R}$ is the vector joining the centers of mass of the collision partners, and $\mathbf{r}$ is the vector between the two clusters.

Inserting Eq. (4) into the full Schrödinger equation of the system and taking a scalar product with each of the intrinsic states, one gets the set of $N+1$ coupled equations

$$\left[E_n - H_{nn}(\mathbf{R})\right]\,\psi_{\rm n}(\mathbf{R}) = \sum_{m=0,m\neq n}^{N} U_{\rm nm}(\mathbf{R})\,\psi_{\rm m}(\mathbf{R}),$$
$$n=0,...,N, \tag{5}$$

where $E_n = E-\varepsilon_n$ is the relative energy in channel n and $U_{\rm nm}(\mathbf{R})$ are the matrix elements of the total projectile-target interaction. These matrix elements are written as

$$U_{nm}(\mathbf{R}) = V_{nm}(\mathbf{R}) - i\,W_{nm}(\mathbf{R}), \tag{6}$$

with

$$V_{nm}(\mathbf{R}) = \int d^3\mathbf{r}\,\phi_n^*(\mathbf{r})\ \mathbb{V}(\mathbf{R},\mathbf{r})\ \phi_m(\mathbf{r}) \tag{7}$$

$$W_{nm}(\mathbf{R}) = \int d^3\mathbf{r}\,\phi_n^*(\mathbf{r})\ \mathbb{W}(\mathbf{R},\mathbf{r})\ \phi_m(\mathbf{r}). \tag{8}$$

The expectation value of $\mathbb{V}(\mathbf{R},\mathbf{r})$ concerning the ground state of the projectile plays the role of the real part of the optical potential in the elastic channel,

$$V_{00}(R) = \int d^3\mathbf{r}\,|\phi_0(\mathbf{r})|^2\ \mathbb{V}(\mathbf{R},\mathbf{r}), \tag{9}$$

where $\phi_0(\mathbf{r})$ is the ground-state wave function of the projectile. A similar potential is obtained for the other channels by changing the g.s. wave function by the wave function of the corresponding state of the projectile. Throughout this paper, we use the São Paulo potential [17, 18] for the real part of the nuclear interactions between the two clusters and the target ($\mathbb{V}^{(1)}$ and $\mathbb{V}^{(2)}$).

The imaginary part of the optical potential in Eq. (2), must account for both the CF and ICF processes. To satisfy the latter requirement, the imaginary potential within the continuum discretized space must have the general form

$$\mathbb{W}(\mathbf{R},\mathbf{r}) = \mathbb{W}^{(1)}(r_1) + \mathbb{W}^{(2)}(r_2). \tag{10}$$

Above, $r_i\,(i=1,2)$ is the distance between the cluster c_i and the target, and the imaginary potential $\mathbb{W}^{(i)}(r_i)$ accounts for the absorption of the cluster c_i by the target. These potentials were parametrized by the short-range Woods-Saxon functions

$$\mathbb{W}^{(i)}(r_i) = \frac{W_0}{1+\exp\left[\left(r_i - R_{\rm w}^{(i)}\right)/a_w\right]}, \qquad i=1,2, \tag{11}$$

with the parameters: $W_0 = 50$ MeV, $r_{\rm w} = 1.0$ fm, and $a_w = 0.2$ fm.

However, it has been shown [16] that this potential leads to wrong CF cross sections at sub-barrier energies. The long tail of the g.s. wave function of ^{6}Li leads to absorption at large distances, which cannot be associated with CF (a detailed discussion of this issue can be found in Ref. [16]). This problem is eliminated by adopting a different potential in the space of bound channels (only the elastic channel in the case of ^{6}Li). In this space, we use the imaginary potential,

$$W^{\rm PT}(R) = \frac{W_0}{1+\exp\left[(R-R_{\rm w})/a_w\right]}, \tag{12}$$

where $R_{\rm w} = r_{\rm w}(A_1^{1/3}+A_2^{1/3})$, with the parameters $W_0 = 100$ MeV, $r_{\rm w} = 1.0$ fm, and $a_w = 0.2$ fm. This potential, which is diagonal in channel space, accounts for the absorption of the whole projectile by the target, ignoring the cluster structure of the projectile.

Thus, we use the imaginary potential of Eqs. (10) and (11) to evaluate matrix elements of the imaginary potential between CDCC bins, and the one of Eq. (12) to evalu-

CPC Accepted

ate the diagonal matrix-element in the elastic channel. As in Refs. [15, 16, 30], we neglect matrix elements of the imaginary potential between bound and unbound channels. This is the approximation of our method. We do not have any physical meaning for these couplings concerning the fusion cross sections (they do not correspond to CF nor to ICF). For consistency, we do not consider these couplings in the CDCC calculations.

The projectile's Hamiltonian of Eq. (2) is

$$h(\mathbf{r}) = -\frac{\hbar^2}{2\mu_{12}}\nabla^2_{\mathbf{r}} + v_{12}(r), \tag{13}$$

where $\mu_{12} = m_0 A_1 A_2/(A_1 + A_2)$ is the relative motion reduced mass. m_0 is the nucleon mass, and A_1, A_2 are the cluster masses. For the $v_{12}(r)$ potential, Woods-Saxon function is usually used in CDCC calculations. Its parameters are varied to reproduce the binding energy of the ground state, and the position and width of the main resonances. We adopted the parameters of Ref. [16].

The projectile-target interaction was expanded in multipoles, keeping multipolarities up to $\lambda_{\max} = 4$. The continuum was discretized using the binning method considering orbital angular momenta between clusters up to $l_{\max} = 3\hbar$. The discretization was performed in the energy space and finer meshes were used around sharp resonances. The ^{6}Li g.s. state is a 1^{+} with $j = 1\hbar$ and $l = 0\hbar$. For more details see Ref. [16].

From CDCC calculations, one obtains the following cross sections:

$$\sigma_{DCF} = \frac{\pi}{K^2}\sum_J (2J+1)\mathcal{P}^{DCF}(J), \tag{14}$$

$$\sigma_F^{(1)} = \frac{\pi}{K^2}\sum_J (2J+1)\mathcal{P}^{(1)}(J), \tag{15}$$

$$\sigma_F^{(2)} = \frac{\pi}{K^2}\sum_J (2J+1)\mathcal{P}^{(2)}(J), \tag{16}$$

where $\mathcal{P}^{DCF}$ corresponds to the probability of the absorption of the whole projectile from the g.s. $\mathcal{P}^{(i)}$ is the probability of absorption of fragment c_i following the breakup. The expressions for these probabilities are given in the appendices of Ref. [30]. Above, $\sigma_F^{(i)}$ corresponds to the inclusive cross section of the fragment c_i, independent of what occurs with the other cluster which does not match with the measurements of the exclusive experiments.

To determine the SCF or ICF cross sections, it is necessary to introduce a model which relates $\mathcal{P}^{(1)}(J)$ and $\mathcal{P}^{(2)}(J)$ to ICF and SCF probabilities. Following the prescription of Ref. [16], we treat $\mathcal{P}^{(1)}(J)$ and $\mathcal{P}^{(2)}(J)$ as probabilities of independent events, and using classical statistics, one introduces

$$\mathcal{P}^{ICF1}(J) = \mathcal{P}^{(1)}(J)\times\left[1 - \mathcal{P}^{(2)}(J)\right], \tag{17}$$

$$\mathcal{P}^{ICF2}(J) = \mathcal{P}^{(2)}(J)\times\left[1 - \mathcal{P}^{(1)}(J)\right], \tag{18}$$

$$\mathcal{P}^{SCF}(J) = \mathcal{P}^{(1)}(J)\times\mathcal{P}^{(2)}(J). \tag{19}$$

To determine the DCF, SCF and the contribution of each fragment to the ICF cross section, we use CF-ICF computer code (unpublished), which evaluates the projected angular momentum version of the expressions derived in Appendix A of Ref. [30]. These expressions involve intrinsic states of the projectile and scattering wave functions obtained by running the CDCC version of the code FRESCO [31]. The theoretical cross sections for the different fusion processes involving the absorption from continuum states are then given by,

$$\sigma_{SCF} = \frac{\pi}{K^2}\sum_J (2J+1)\mathcal{P}^{SCF}(J), \tag{20}$$

$$\sigma_{ICF1} = \frac{\pi}{K^2}\sum_J (2J+1)\mathcal{P}^{ICF1}(J), \tag{21}$$

$$\sigma_{ICF2} = \frac{\pi}{K^2}\sum_J (2J+1)\mathcal{P}^{ICF2}(J). \tag{22}$$

The ICF cross section is the sum of the corresponding quantity for each cluster, i.e.

$$\sigma_{ICF} = \sigma_{ICF1} + \sigma_{ICF2}. \tag{23}$$

The CF and TF cross sections are defined by

$$\sigma_{CF} = \sigma_{DCF} + \sigma_{SCF}, \tag{24}$$

$$\sigma_{TF} = \sigma_{CF} + \sigma_{ICF}. \tag{25}$$

We use this method in the present work to study fusion reactions in collisions of ^{6}Li projectile with ^{209}Bi target, for which there are experimental data available in Ref. [14], and new measurements were performed in this work using different experimental techniques.

CPC Accepted

V. DISCUSSION

Now we use the theoretical model of Ref. [16] to analyze the data of the present work and other fusion data available in the literature for the same system.

A. CF cross sections

Figure 5 shows the CF data of the present work in comparison with the data of Dasgupta *et al*. [14] and the CDCC predicted cross section of Ref. [16]. The figure also shows the fusion cross section predicted by the barrier penetration model (BPM) with the São Paulo potential for the ^{6}Li + ^{209}Bi system, neglecting the cluster structure of ^{6}Li. We observe that the CF data of the present work agree very well with the data of Dasgupta *et al*. [14], and also with the cross section predicted by CDCC. On the other hand, the experimental cross sections are larger than the BPM cross section at sub-barrier energies. But at energies above the Coulomb barrier, the experimental results are smaller than that of BPM.

The validity of the CDCC calculation can also be checked by comparing the theoretical and experimental CF barrier distributions [32],

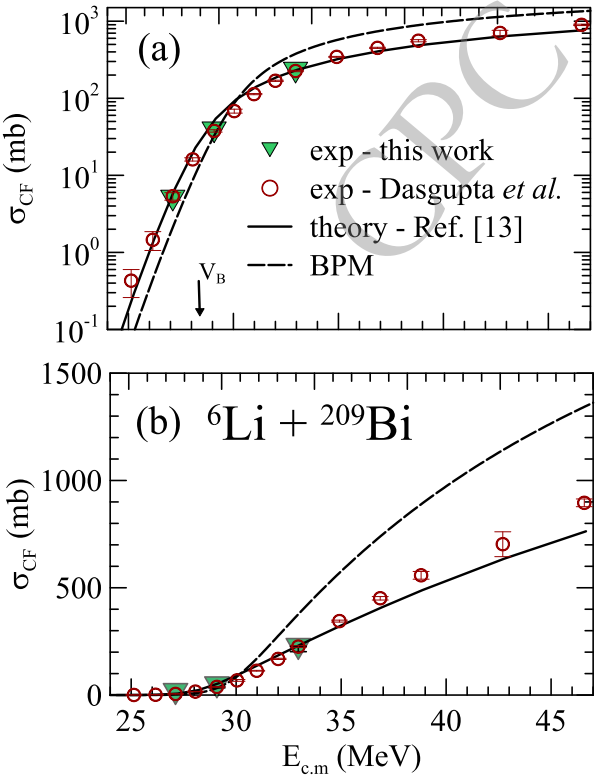

Fig. 5. (color online) Theoretical CF cross section in collision of ^{6}Li with target ^{209}Bi. The cross section calculated by our model is compared with the data of Refs.[13, 14](^{6}Li +^{209}Bi) and the present measurements. Besides, the dashed line shows the results obtained considering the BPM approach.

$$D_{\rm CF}(E) = \frac{d^2(E\sigma_{\rm CF})}{dE^2}, \tag{26}$$

where E is the collision energy in the center-of-mass frame. In the present work, the theoretical barrier distribution was evaluated by the 3-points formula, based on the Taylor expansion of $E\sigma_{CF}(E)$, using the mesh step and the detailed procedure can be found in Ref. [33]. Here, the experimental data were solely taken from Ref. [14] since the current new data only cover three energies, reasonably coinciding with the previous ones.

From the comparison as shown in Fig. 6, one observes that the CDCC calculation slightly underestimates the experimentally measured barrier distribution, which is more obvious for the high-energy region (beam energy greater than 30 MeV as shown in Fig. 6). This phenomenon is consistent with the situation in Fig. 5(b) where the CDCC slightly underestimates the measured CF cross sections. The possible reasons could be (1) the barrier (V_{00} as mentioned in Eq.(9)) might be too attractive, especially when assuming the breakup coupling is considered correctly in the current CDCC calculation, or (2) the V_{00} is correct, but the calculated ICF cross section with the same barrier is too large. The second reason seems reasonable if one only checks the comparison for ICF cross sections in the following subsection. However, the conclusion cannot be fixed at the current stage since the obtained cross sections for ICF are only the lower bound due to the difficulties on the experimental side, as mentioned in the introduction and the detailed experimental sections. Due to the limitation of the in-beam γ-ray measurement method, we were unable to obtain the counts of some γ-rays with very weak intensity since they are so overwhelmed by the background, then it is impossible to calculate their yield. Therefore, one gives the lower limit of cross section. Thus, a more conclusive res-

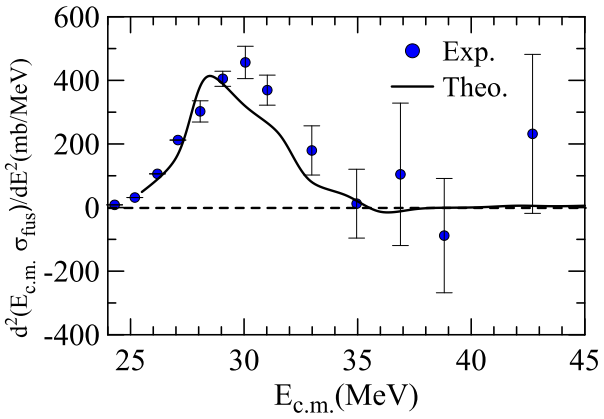

Fig. 6. (color online) Experimental barrier distribution for the ^{6}Li+^{209}Bi complete fusion cross section compared with the theoretical one derived from the theoretical CF cross sections of work.

CPC Accepted

ult demands higher precision measurement in future work.

Concerning the comparison with BPM calculation, a crucial issue in the CF of weakly bound projectiles is the question of hindrance or enhancement in collisions of various targets in different energy regimes. The low binding energies of the clusters give rise to a long tail in the g.s. wave function of the projectile. This effect leads to a lower Coulomb barrier, which enhances the fusion cross section at all collision energies. On the other hand, the low breakup threshold leads to strong couplings with the breakup channels. These couplings give rise to ICF, suppressing CF. The behavior of the CF data is dictated by the competition of these two opposite tendencies.

Figure 7 shows the Coulomb barriers associated with the nuclear potential that considers the cluster structure of ^{6}Li and the one that neglects it. The former, denoted by $V_{00}(R)$, is the expectation value of the potential of Eq. (3) with respect to the g.s. wave function of ^{6}Li (see Eq. (9)). The latter is the standard São Paulo Potential for the ^{6}Li + ^{209}Bi system, denoted by $V_{\rm PT}(R)$. The barrier parameters of the two potentials are given in Table 3. In this case, the low binding energy of the clusters leads to the barrier lowering $\Delta V_{\rm B} \equiv V_{\rm B}^{\rm PT} - V_{\rm B}^{00} = 1.6$ MeV.

Systematic studies of suppression and enhancement of CF in collisions of weakly bound projectiles are usually carried out regarding reduced cross sections. The reduction procedure aims at eliminating trivial differences in the cross sections arising from the charges and sizes of the collision partners (a review of these methods can be found in Ref. [34]). We adopt here the fusion function reduction method proposed by Canto *et al.* [35, 36]. The method consists of transformations,

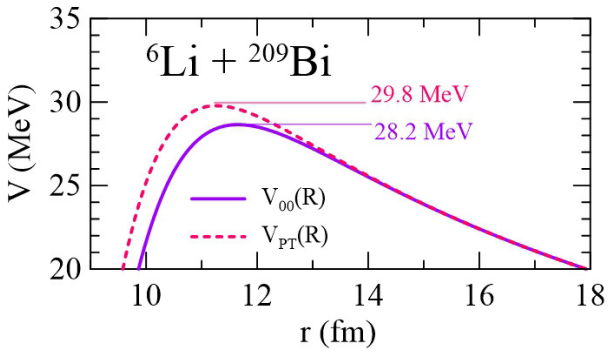

Fig. 7. (color online) Coulomb barriers of the potentials $V_{\rm PT}(R)$ and $V_{00}(R)$ obtained for the ^{6}Li +^{209}Bi system.

Table 3. Barrier parameters for the potentials $V_{00}(R)$ and $V_{\rm PT}(R)$ for the system study in this work.

Potential/Parameter	R_B (fm)	V_B (MeV)	$\hbar\omega$ (MeV)
$V_{\rm PT}(R)$	11.3	29.8	4.8
$V_{00}(R)$	11.8	28.2	4.4

$$x = \frac{E_{\rm c.m.} - V_{\rm B}}{\hbar\omega} \quad \text{and} \quad F(x) = \frac{2E_{\rm c.m.}}{\hbar\omega R_{\rm B}^2}\,\sigma_{\rm F}, \tag{27}$$

where $R_{\rm B}, V_{\rm B}$, and $\hbar\omega$ are the parameters of the parabolic approximation to the Coulomb barrier. The reduced cross section, $F(x)$, is the fusion function associated with the cross section $\sigma_{\rm F}$. In an ideal situation where there are no channel coupling effects and the one-channel fusion cross section is well described by the Wong formula [37], $F(x)$ reduces to the universal fusion function (UFF), given by

$$F_0(x) = \ln\left[1 + \exp(2\pi x)\right]. \tag{28}$$

Thus, $F(x)$ deviations with respect to the UFF may indicate that channel couplings influence the fusion cross section. However, they may also indicate that the Wong formula is invalid in the corresponding energy region. It is well known (see e.g., Refs. [1, 36]) that the Wong formula overestimates the one-channel cross section of light and intermediate-mass systems ($Z_{\rm P} \times Z_{\rm T} < 500$) at sub-barrier energies. Then, to reach any reliable conclusion about the influence of nuclear structure properties, this possibility must be discarded. This can be achieved by replacing $F(x)$ with a renormalized fusion function, defined as

$$\overline{F}(x) = F(x) \times \frac{\sigma_W}{\sigma_{BPM}}. \tag{29}$$

To evaluate the renormalized fusion function associated with the experimental cross section, $\overline{F}_{\rm exp}(x)$, one has to select a reference potential. This potential gives the barrier parameters appearing in Eq. (27), and the BPM cross section in Eq. (29). The first possibility is to use the standard São Paulo potential for the ^{6}Li + ^{209}Bi system, $V_{\rm PT}(R)$. Another possibility is to adopt the potential $V_{00}(R)$. The fusion functions evaluated with these potentials are denoted by $\overline{F}_{\rm exp}^{\rm PT}(x)$ and $\overline{F}_{\rm exp}^{00}(x)$, respectively. A detailed discussion of these fusion functions is presented below.

Since the potential $V_{\rm PT}(R)$ completely ignores the cluster structure of ^{6}Li, comparing $\overline{F}_{\rm exp}^{\rm PT}(x)$ with the UFF, we can assess the net effect of the low binding energy of the clusters in ^{6}Li. That is, the result of the competition between the enhancement arising from the barrier lowering against the suppression resulting from breakup couplings. The results are shown in logarithmic (Fig. 8(a)) and linear (Fig. 8(b)) scales. The first scale is more appropriate for showing the coupling effects below the Coulomb barrier, while the second is for the above barrier energy regime, where the hindrance due to the breakup is usually studied. Compared to UFF, $\overline{F}_{\rm exp}^{\rm PT}(x)$ is enhanced below the Coulomb barrier and suppressed at above-barrier energies. In the lower energy region, the fusion function

CPC Accepted

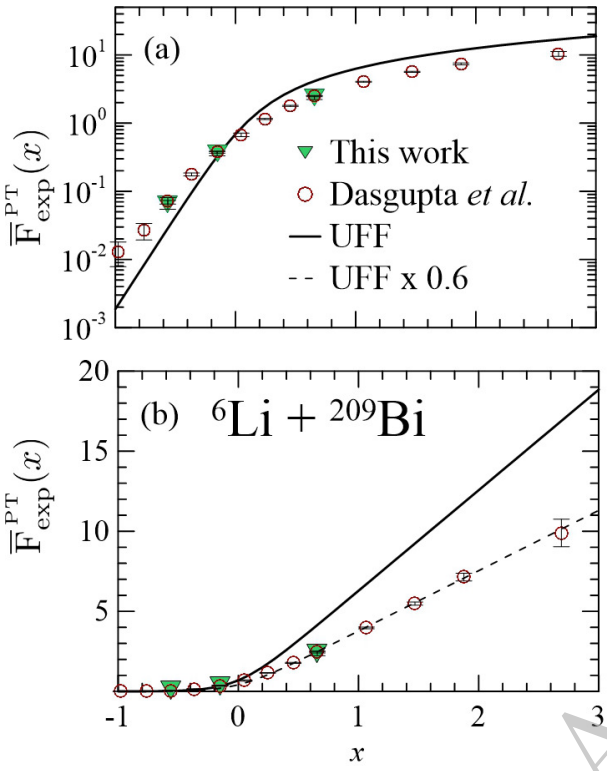

Fig. 8. (color online) Fusion function in the collision of ^{6}Li projectile on a ^{209}Bi target, corresponding to the Ref. [14] data and the present measurements. The barrier parameters are derived from the $V_{PT}(R)$ nuclear potential (see text for details).

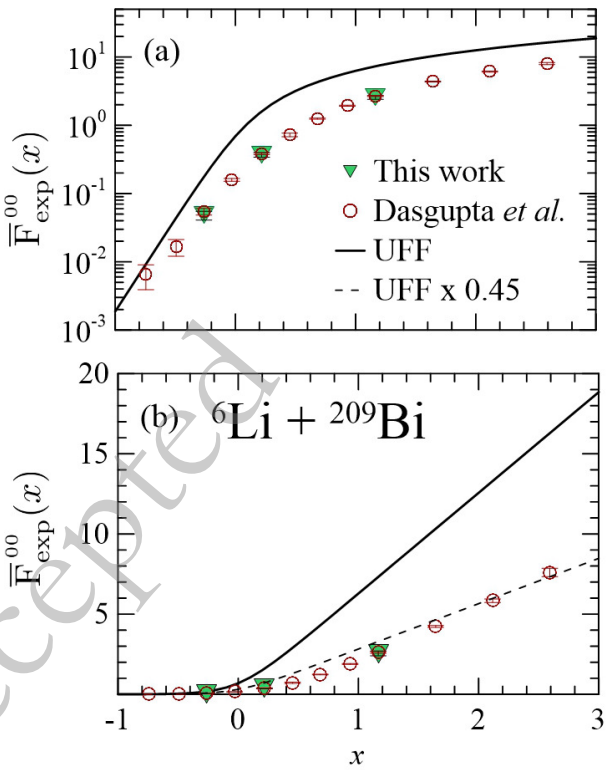

Fig. 9. (color online) Same as Fig. 8 but using $V_{00}(R)$ to derive barrier parameters (see text for details).

is very close to the curve corresponding to the UFF multiplied by the factor 0.6, represented by the dashed line in the linear plot. This indicates that the fusion function is suppressed by 40% {when using $V_{PT}(R)$, being very similar to the result obtained in Ref. [14] in which the experimental barrier is used in the theoretical calculation. It is not a surprising result that the $V_{PT}(R)$ is very close to the measured barrier (30.0 ± 0.3 MeV in Ref. [14]) since the experimental barrier has to consider all the coupling effect. As mentioned before, the competition between the clustering (lowering barrier) against the breakup couplings (increasing barrier) might almost cancel their difference.

Now we consider the fusion function $\overline{F}^{00}_{exp}(x)$. Since the barrier-lowering effects are already contained in the potential $V_{00}(R)$, deviations concerning the UFF result exclusively from the dynamic effects of the breakup couplings. Fig. 9 compares this fusion function with the UFF. As in the previous figure, the results are shown in logarithmic (Fig. 9(a)) and linear (Fig. 9(b)) scales. It is supposed that in this condition, only the suppression arising from breakup couplings remains in the comparison. Thus, the fusion function is suppressed at all collision energies. Above the Coulomb barrier, the fusion function is close to the UFF multiplied by 0.45 (dashed line in the Fig. 9(b)). Thus, there is a suppression of 55%. As expected, the suppression is larger than that exhibited by $\overline{F}^{PT}_{exp}(x)$, which keeps the barrier-lowering effects. This also implies that the real part of dynamic polarization potential produced by the breakup channels is repulsive in the whole energy interval (see Ref. [2] and references therein). It has to be stressed here that we are not saying to change the value of the suppression factor, but the current analysis can help to distinguish the contributions from different coupling effects.

In Ref. [38], a systematic study of breakup effects on complete fusion at energies above the Coulomb barrier was performed. A suppression factor was obtained for experimental CF involving several weakly bound projectiles. The CF was reduced using the fusion function method and the São Paulo potential for the nuclear interaction to derive barrier parameters. The systematic value of the reduction coefficient for reactions induced for the ^{6}Li projectile was 0.6 in agreement, as expected, with the value obtained in the present work when the São Paulo potential was used. To have a larger value for the CF suppression factor when V_{00} is used is only an apparent contradiction. In this last case, the cluster structure of the projectile was considered, allowing for complete isolation of the static effect of breakup on the CF cross section.

To finish this sub-section, we emphasize that al-

CPC Accepted

though experimentally is not possible to separate the DCF and SCF, theoretically, this can be done using expressions (14) and (20). We will not plot these two contributions because it would contribute to our knowledge of the breakup-fusion reaction mechanism only in a very limited way. For that, an extensive study using different targets and projectiles is mandatory. This is out of the scope of the present manuscript.

B. ICF and TF cross sections

Figure 10 shows the ICF data of the present experiment, together with the contribution from the capture of each fragment ($d-$ICF and $\alpha-$ICF). They are compared with the corresponding theoretical cross sections obtained in the Ref. [16] calculations. The solid blue line is the same ICF cross section reported in Ref. [16] (dotted line in panels (g) and (h) of Fig. 6 of this paper). The dashed black line and the dashed-dotted red lines correspond to the theoretical d-ICF and α-ICF cross sections, respectively. These results were not reported in that paper because this kind of data was unavailable then. The experiment method adopted by Dasgupta *et al.* [14] was appropriate for measuring the ICF cross section, but only works when the α decay half-lives of the residues are not so long as mentioned before in the introduction.

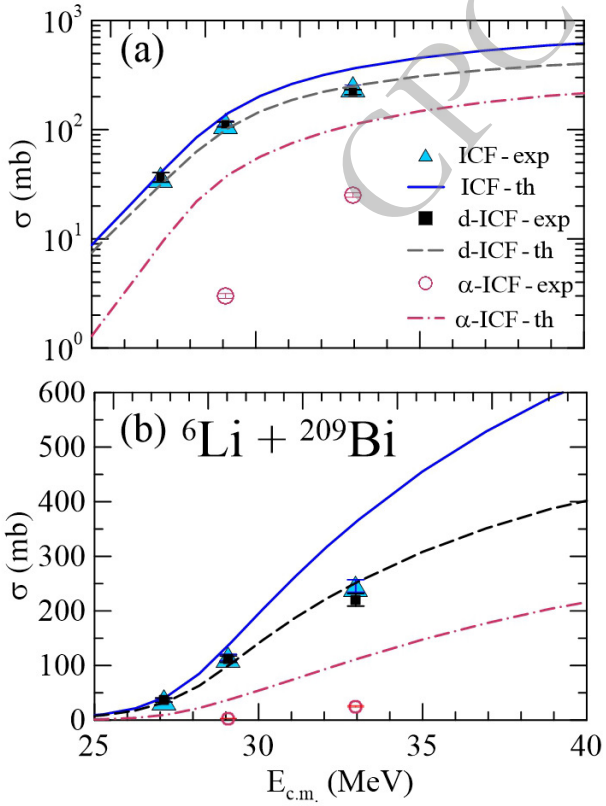

Fig. 10. (color online) Comparison of the experimental data for the incomplete functions for deuteron and α-particle ($d-$ICF and α-ICF) with the theoretical results for the ^{6}Li +^{209}Bi reaction.

By comparing the CF cross section and ICF cross section in Fig. 5 and Fig. 10, it can be found that the ICF cross section is equivalent to the CF cross section at energies above the Coulomb barrier but exceeds the CF cross section below the Coulomb barrier and dominates the TF cross section. In Fig. 2 of Ref. [39], the NEB (non-elastic breakup) cross section, which contains ICF and transfer, similarly exceeds the CF section in the near-barrier energies, which proves the rationality of our results.

Comparing the experimental $d-$ICF cross section with the dashed line, one concludes that the theoretical model fairly describes the data. Conversely, the theoretical prediction of the α-ICF cross section (dash-dotted line) is much larger than the data. However, this comparison is inconclusive. As we pointed out in an earlier section of this paper, the current experimental α-ICF data is just a lower bound for the actual cross section.

Before discussing the TF, we mention that ICF, considered an absorption, is distinguished from cluster transfer from the theoretical point of view. Cluster transfer is one of the contributors to experimental ICF because the products are indistinguishable depending on the possible fragments produced in the reaction. Fusion is understood as a short-range absorption, while transfer is a more peripheral process, so the mechanism should differ. Consequently, specific reaction calculations may or may not explicitly include transfer channels. The CDCC method used in this paper is an example of the latter. At the same time, other models, such as the coupled reaction channel [40] or the Ichimura-Austern-Vincent model [41], include transfer explicitly. Although this is the general case, in Ref. [16], it was shown that the deuteron cluster transfer cross section is much smaller than d-ICF in the whole energy interval studied in the present work. Nevertheless, deuteron cluster transfer was found to be a relevant mechanism for the ^{6}Li + ^{197}Au at energies below the Coulomb barrier.

Figure 11 compares the theoretical TF cross section with the experimental TF cross section of the present work and the one measured by Dasgupta *et al.*. One observes that the theoretical curve is systematically higher than the data points. As mentioned before, our experiment misses parts of α-ICF events that should also contribute to the TF cross section. On the other hand, measurements of Ref. [14] miss the contribution from the α-decay of a long-life isotope, which according to estimates made by the code PACE [10−12], is important in the whole energy interval of the experiment. Nevertheless, in the case of the present experiment, the contribution of the $\alpha-$ICF to the TF at the two lower energies is small, showing quite a good agreement between theory and experiment. We recall that the theoretical TF cross section shown in this work is the one already reported in Ref. [16].

CPC Accepted

In addition to incomplete data for ICF cross section, it should be stressed here that the discrepancy between experiment and theory as shown in Figs. 10 and 11 could also partly come from the ill-definition of total fusion since the cluster transfer and proton transfer reaction can also contribute to the ICF and TF cross section. Thus, a more comprehensive study, including a new complete measurement compared with a more sophisticated model, is required to solve this problem in the future.

VI. SUMMARY

The experiment ^{6}Li+^{209}Bi has been performed at the Tandem-XTU accelerator of INFN-LNL, Italy. The CF and ICF cross sections for the ^{6}Li+^{209}Bi system at near-Coulomb barrier energies were obtained by in-beam γ measurements. The experimental results demonstrated that the ICF cross section is of the same order as the CF cross section above the Coulomb barrier and dominates at energies around and below the Coulomb barrier.

A theoretical approach based on the CDCC method was employed to describe the same system, and the calculated CF cross sections agree well with the experimental results, especially for the *d*-ICF ones. The fusion function method is employed to assess the impact of breakup on the fusion process. It was found that the CF reduction factor is quite sensitive to the choice of potential and related barrier parameters, demanding more accurate data for total fusion cross section.

It is relevant to point out that above a certain threshold, the deuteron can break up, and the ^{6}Li projectile would be more reasonably described by $\alpha+n+p$ configuration. This configuration is not accessible at low beam energies but could be relevant at higher energies. It would be interesting to check this possibility within the four-body CDCC calculations above the $n+p$ threshold. Another possibility would be a sequential breakup of the projectile. So, firstly, the ^{6}Li breaks up into $\alpha+d$, and in the second step, the deuteron breaks up into $n+p$. These are some of our plans for developing our theoretical model.

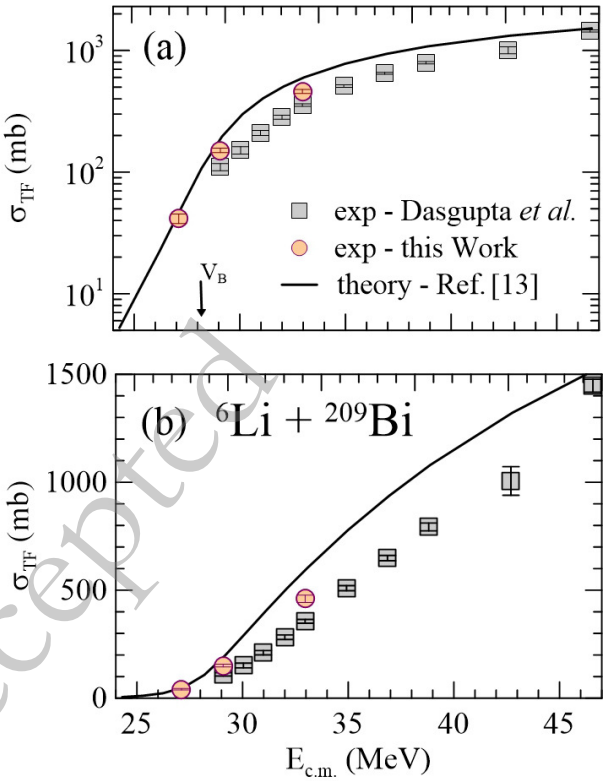

Fig. 11. (color online) Comparison theoretical TF cross section for the ^{6}Li +^{209}Bi system with the available experimental data.

CPC Accepted

ACKNOWLEDGMENTS

We are grateful to the INFN-LNL staff for providing a stable ^{6}Li beam throughout the experiment. Brazilian authors thank the partial financial support from CNPq, FAPERJ, and INCT-FNA (Instituto Nacional de Ciência e Tecnologia, Física Nuclear e Aplicações), research Project No. 464898/2014-5.

References

[1] L. F. Canto, P. R. S. Gomes, R. Donangelo, and M. S. Hussein, Phys. Rep. **424**, 1 (2006)
[2] L. F. Canto, P. R. S. Gomes, R. Donangelo, J. Lubian, and M. S. Hussein, Phys. Rep. **596**, 1 (2015)
[3] M. Ray, A. Mukherjee, M. K. Pradhan, R. Kshetri, M. S. Sarkar, R. Palit, I. Majumdar, P. K. Joshi, H. C. Jain, and B. Dasmahapatra, Phys. Rev. C **78**, 064617 (2008)
[4] M. Sinha, H. Majumdar, P. Basu, S. Roy, R. Bhattacharya, M. Biswas, M. K. Pradhan, and S. Kailas, Phys. Rev. C **78**, 027601 (2008)
[5] S. P. Hu, G. L. Zhang, J. C. Yang, H. Q. Zhang, P. R. S. Gomes, J. Lubian, X. G. Wu, J. Zhong, C. Y. He, Y. Zheng, C. B. Li, G. S. Li, W. W. Qu, F. Wang, L. Zheng, L. Yu, Q. M. Chen, P. W. Luo, H. W. Li, Y. H. Wu, W. K. Zhou, B. J. Zhu, and H. B. Sun, Phys. Rev. C **91**, 044619 (2015)
[6] F. Gollan, D. Abriola, A. Arazi, M. A. Cardona, E. de Barbará, J. de Jes′us, D. Hojman, R. M. I. Betan, J. Lubian, A. J. Pacheco, B. Paes, D. Schneider, and H. O. Soler, Phys. Rev. C **104**, 024609 (2021)
[7] A. Shrivastava, A. Navin, A. Lemasson, K. Ramachandran, V. Nanal, M. Rejmund, K. Hagino, T. Ishikawa, S. Bhattacharyya, A. Chatterjee, S. Kailas, K. Mahata, V. V. Parkar, R. G. Pillay, and P. C. Rout, Phys. Rev. Lett. **103**, 232702 (2009)
[8] L. R. Gasques, D. J. Hinde, M. Dasgupta, A. Mukherjee, and R. G. Thomas, Phys. Rev. C **79**, 034605 (2009)
[9] M. Dasgupta, D. J. Hinde, S. L. Sheehy, and B. Bouriquet, Phys. Rev. C **81**, 024608 (2010)

[10] A. Gavron, Phys. Rev. C **21**, 230 (1980)
[11] O. Tarasov and D. Bazin, Nucl. Phys. A **746**, 411 (2004)
[12] "Pace 4 : Gui evaporation code (win, macos, linux), " Online (2024).
[13] M. Dasgupta, D. J. Hinde, K. Hagino, S. B. Moraes, P. R. S. Gomes, R. M. Anjos, R. D. Butt, A. C. Berriman, N. Carlin, C. R. Morton, J. O. Newton, and A. Szanto de Toledo, Phys. Rev. C **66**, 041602(R) (2002)
[14] M. Dasgupta, P. R. S. Gomes, D. J. Hinde, S. B. Moraes, R. M. Anjos, A. C. Berriman, R. D. Butt, N. Carlin, J. Lubian, C. R. Morton, J. O. Newton, and A. Szanto de Toledo, Phys. Rev. C **70**, 024606 (2004)
[15] J. Rangel, M. Cortes, J. Lubian, and L. F. Canto, Phys. Lett. B **803**, 135337 (2020)
[16] J. Lubian, J. L. Ferreira, J. Rangel, M. R. Cortes, and L. F. Canto, Phys. Rev. C **105**, 054601 (2022)
[17] L. C. Chamon, D. Pereira, M. S. Hussein, M. A. Candido Ribeiro, and D. Galetti, Phys. Rev. Lett. **79**, 5218 (1997)
[18] L. C. Chamon, B. V. Carlson, L. R. Gasques, D. Pereira, C. De Conti, M. A. G. Alvarez, M. S. Hussein, M. A. C?andido Ribeiro, E. S. Rossi Jr., and C. P. Silva, Phys. Rev. C **66**, 014610 (2002)
[19] A. Goasduff, D. Mengoni, F. Recchia, J. Valiente-Dobon, R. Menegazzo, G. Benzoni, D. Barrientos, M. Bellato, N. Bez, M. Biasotto, *et al.*, Nucl. Instr. and Meth. Phys. Res. A **1015**, 165753 (2021)
[20] D. Testov, D. Mengoni, A. Goasduff, A. Gadea, R. Isocrate, P. R. John, G. de Angelis, D. Bazzacco, C. Boiano, A. Boso, *et al.*, Eur. Phys. J. A **55**, 47 (2019)
[21] P. M. Davidson, G. D. Dracoulis, A. P. Byrne, T. Kibédi, B. Fabricius, A. M. Baxter, A. E. Stuchbery, A. R. Poletti, and K. J. Schiffer, Nucl. Phys. A **560**, 822 (1993)
[22] C. B. Li, G. L. Zhang, C. X. Yuan, G. X. Zhang, S. P. Hu, W. W. Qu, Y. Zheng, H. Q. Zhang, D. Mengoni, D. Testov, *et al.*, Phys. Rev. C **101**, 044313 (2020)
[23] L. J. Jardine, S. G. Prussin, and J. M. Hollander, Nucl. Phys. A **233**, 25 (1974)
[24] L. G. Mann, K. Maier, A. Aprahamian, J. A. Becker, D. J. Decman, E. A. Henry, R. A. Meyer, N. Roy, W. Stöffl, and G. L. Struble, Phys. Rev. C **38**, 74 (1988)
[25] I. Bergström, B. Fant, C. Herrlander, P. Thieberger, K. Wikström, and G. Astner, Phys. Lett. B **32**, 476 (1970)
[26] T. Lönnroth, V. Rahkonen, and B. Fant, Nucl. Phys. A **376**, 29 (1982)
[27] L. F. Canto, R. Donangelo, M. S. Hussein, P. Lotti, J. Lubian, and J. Rangel, Phys. Rev. C **98**, 044617 (2018)
[28] Y. Sakuragi, M. Yahiro, and M. Kamimura, Prog. Theoret. Phys. Suppl. **89**, 136 (1986)
[29] N. Austern, Y. Iseri, M. Kamimura, M. Kawai, G. Rawitscher, and M. Yashiro, Phys. Rep. **154**, 125 (1987)
[30] M. R. Cortes, J. Rangel, J. L. Ferreira, J. Lubian, and L. F. Canto, Phys. Rev. C **102**, 064628 (2020)
[31] I. J. Thompson, Comput. Phys. Rep. **7**, 167 (1988)
[32] N. Rowley, G. Satchler, and P. Stelson, Phys. Lett. B **254**, 25 (1991)
[33] L. Canto and R. Donangelo, Phys. Rev. C **79**, 037601 (2009)
[34] L. F. Canto, D. R. Mendes Junior, P. R. S. Gomes, and J. Lubian, Phys. Rev. C **92**, 014626 (2015)
[35] L. F. Canto, P. R. S. Gomes, J. Lubian, L. C. Chamon, and E. Crema, Nucl. Phys. A **821**, 51 (2009)
[36] L. F. Canto, P. R. S. Gomes, J. Lubian, L. C. Chamon, and E. Crema, J. Phys. G: Nucl. Part. Phys. **36**, 015109 (2009)
[37] C. Y. Wong, Phys. Rev. Lett. **31**, 766 (1973)
[38] B. Wang, W.-J. Zhao, P. R. S. Gomes, E.-G. Zhao, and S.-G. Zhou, Phys. Rev. C **90**, 034612 (2014)
[39] J. Lei and A. M. Moro, Phys. Rev. Lett. **122**, 042503 (2019)
[40] I. J. Thompson, Comput. Phys. Rep. **7**, 167 (1988)
[41] J. Lei and A. M. Moro, Phys. Rev. Lett. **122**, 042503 (2019)

CPC Accepted